

Critical behavior of a colloid-polymer mixture confined between walls

R. L. C. Vink

*Institut Theoretische Physik II, Heinrich Heine Universität,
Universitätsstraße 1, 40225 Düsseldorf, Germany*

K. Binder and J. Horbach

*Institut für Physik, Johannes Gutenberg-Universität, Staudinger Weg 7, 55099 Mainz, Germany
(Dated: May 7, 2022)*

We investigate the influence of confinement on phase separation in colloid-polymer mixtures. To describe the particle interactions, the colloid-polymer model of Asakura and Oosawa [J. Chem. Phys. **22**, 1255 (1954)] is used. Grand canonical Monte Carlo simulations are then applied to this model confined between two parallel hard walls, separated by a distance $D = 5$ colloid diameters. We focus on the critical regime of the phase separation and look for signs of crossover from three-dimensional (3D) Ising to two-dimensional (2D) Ising universality. To extract the critical behavior, finite size scaling techniques are used, including the recently proposed algorithm of Kim *et al.* [Phys. Rev. Lett. **91**, 065701 (2003)]. Our results point to “effective” critical exponents that differ profoundly from 3D Ising values, and that are already very close to 2D Ising values. In particular, we observe that the critical exponent β of the order parameter in the confined system is smaller than in 3D bulk, yielding a “flatter” binodal. Our results also show an increase in the critical colloid packing fraction in the confined system with respect to the bulk. The latter seems consistent with theoretical expectations, although subtleties due to singularities in the critical behavior of the coexistence diameter cannot be ruled out.

PACS numbers: 05.70.Jk, 64.60.Fr, 64.70.Fx

I. INTRODUCTION

The current technological demand for the production of nanoscopic devices [1, 2, 3, 4, 5] renewed the interest in understanding the phase behavior of fluid systems confined in pores of nanoscopic linear dimensions [6, 7]. In addition, porous materials with pore widths less than 50 nm are widely used in the chemical, oil and gas, food, and pharmaceutical industries, for applications such as mixture separation, pollution control, and as catalysts [6, 8, 9, 10]. However, many such applications rely largely on empirical knowledge, since the theory-based understanding of confined fluids is still rather incomplete [6, 11, 12, 13, 14, 15]. Even the basic phenomenon of “capillary condensation” of undersaturated gases in capillaries, described already in the 19th century [16], still forms the subject of longstanding investigations by analytical theory [17, 18, 19, 20, 21, 22, 23, 24, 25] and computer simulations [20, 26, 27, 28, 29, 30, 31, 32, 33, 34, 35]. Regarding confined binary mixtures, there is a close analogy between the phase behavior of confined one-component fluids and the preferential adsorption of one of the components of the mixture to the walls. The miscibility gap of the mixture corresponds to the coexistence curve (or binodal) that describes the phase separation between liquid and gas in simple fluids, and numerous theoretical and simulational studies have addressed the phase behavior of binary mixtures in cylindrical pores or slit pores [36, 37, 38, 39, 40, 41, 42, 43, 44, 45, 46, 47]. Depending on the details of the wall-particle interactions in relation to the interactions among the fluid particles of a binary (AB) mixture, it is clear that there can be

either the A-component or the B-component attracted to the walls, apart from the very special case of “neutral walls” which produce confinement only [48, 49, 50]. Similarly, in a one-component liquid-gas system “capillary evaporation” [46, 51, 52, 53] can occur for repulsive wall-particle interactions. While for the liquid-gas transition and the demixing transition of binary fluids the “order parameter” of the transition is a simple scalar, i.e. the transition belongs to the “universality class” of the Ising (lattice gas) model [54], related phenomena occur in systems with more complex ordering, e.g. confined liquid crystals where “capillary nematization” may occur [55].

Understanding nanoscopic confinement of fluids consisting of small molecules is difficult because the lateral variation of the wall potential, due to wall roughness or even atomistic corrugation [56] of the wall potential, may have drastic effects on the phase behavior of the confined fluid [57]. In this respect, colloidal systems due to the mesoscopic size of the colloidal particles pose distinct advantages: atomistic corrugation of the confining wall potentials can safely be neglected, and there is a great freedom in preparing systems with suitable interactions [58, 59, 60]. A particularly suitable class of systems are colloid-polymer mixtures, since both bulk phase behavior and the interfaces separating the colloid-rich and polymer-rich phases can be studied experimentally in detail [61, 62, 63, 64]. Furthermore, the Asakura-Oosawa (AO) model [65, 66] provides a simple theoretical description, which seems to capture all the salient features of such phase-separating colloid-polymer mixtures, and which is well suited to computer simulation investigations [46, 67, 68, 69].

Therefore, we use this model again in the present pa-

per to address the question: how does the critical behavior near the demixing critical point change due to the confinement in slit pores? While on general theoretical grounds one expects [15, 18, 34, 35, 48, 49, 50] that in the ultimate vicinity asymptotically close to the critical point the critical exponents of the two-dimensional (2D) Ising model should apply [70], this limiting asymptotic behavior may be hard to observe, and the need arises to consider the crossover from three dimensional (3D) to two-dimensional critical behavior in such thin films [48, 49, 50]. This crossover behavior in itself is a difficult but interesting problem [49]. Previous work considering this issue has been restricted to either simple Ising (lattice gas) models [18, 35, 48] or strictly symmetric polymer mixtures confined by neutral walls [50]. The complications due to the asymmetry between liquid(-like) and gas(-like) phases in the bulk have not been considered, and also the further asymmetry arising from the preferential adsorption of one species to the walls has been disregarded. Due to this preferential adsorption, one expects near the critical point of the bulk the formation of wetting layers at the walls [15, 71, 72, 73, 74] if the width of the slit pore becomes very large.

We note that previous theoretical work on capillary condensation (or evaporation) based on density functional theory (DFT), or other analytical approximations for the equation of state, inevitably implies a parabolic shape of the binodal near the critical value $\eta_{p,cr}^r$ of the polymer reservoir packing fraction η_p^r , irrespective of whether one considers the bulk mixture or a confined system. Therefore, despite the fact that such theories are very powerful away from the critical point, they cannot be used to describe the crossover in the critical behavior due to confinement. Also previous Gibbs ensemble simulations of the AO model confined to slit pores [46] did not address this issue since the Gibbs ensemble cannot be used to sample the critical point. In the present work, we therefore extend the *grand canonical* techniques used in our previous work on the critical behavior of the AO model in the bulk [67, 68] to study the critical behavior in confinement.

The outline of this paper is as follows. In Section II, we briefly review crossover scaling relations that are expected to describe the critical behavior of a confined fluid. Next, we introduce the AO model and describe our simulation method. In Section III, we present our results, using a finite size scaling analysis of the critical properties for a very thin film of thickness $D = 5\sigma_c$, with σ_c the diameter of the hard-sphere colloids. We end with a summary and conclusion in the last section.

II. CROSSOVER SCALING

To define the problem of study more precisely, we recall that the width of the binodal, or order parameter, of a colloid-polymer mixture is given by

$$\Delta \equiv (\eta_c^l - \eta_c^v)/2, \quad (1)$$

with η_c^l (η_c^v) the colloid packing fraction in the colloidal liquid (vapor) phase. In 3D bulk, the order parameter close to the critical point is expected to scale as

$$\Delta(\infty) = \hat{B}t_\infty^\beta, \quad t_\infty \equiv \eta_p^r/\eta_{p,cr}^r(\infty) - 1, \quad (2)$$

where \hat{B} is a (nonuniversal) critical amplitude, and $\beta \approx 0.326$ the (universal) critical exponent of the 3D Ising universality class [54, 75, 76]. The symbol (∞) in the above emphasizes that $\eta_{p,cr}^r$ is the critical value of the polymer reservoir packing fraction appropriate for an infinitely thick film, i.e. a bulk 3D system.

In a confined thin film of thickness D , however, the corresponding relation reads

$$\Delta(D) = \hat{B}(D)t_D^{\beta_2}, \quad t_D \equiv \eta_p^r/\eta_{p,cr}^r(D) - 1. \quad (3)$$

The critical polymer reservoir packing fraction is thus shifted from its bulk value $\eta_{p,cr}^r(\infty)$ to a new value $\eta_{p,cr}^r(D)$. In addition, the critical amplitude $\hat{B}(D)$ depends on the film thickness D , and the critical exponent takes the value of the 2D Ising universality class $\beta_2 = 1/8$ [54, 70]. However, as D gets large, the validity of Eq.(3) is expected to be observable only in an extremely narrow region around $t_D = 0$. This is recognized when one formulates the appropriate crossover scaling description [18, 35, 48, 50, 77]

$$\Delta = D^{-\beta/\nu} F(D^{1/\nu}t_\infty), \quad (4)$$

where ν is the critical exponent of the correlation length for the 3D Ising universality class [54, 75, 76], and $F(X)$ a crossover scaling function with $X \equiv D^{1/\nu}t_\infty$. Eq.(4) may qualitatively be interpreted using the finite size scaling principle [78, 79, 80, 81] in which the film thickness D scales with the correlation length $\xi = \hat{\xi}t_\infty^{-\nu}$, where $\hat{\xi}$ is another critical amplitude. To recover Eq.(2) from Eq.(4), one notes that the scaling function $F(X)$ must behave as $F(X) \propto X^\beta$ for $X \rightarrow \infty$. At a fixed small value of t_∞ , the D -dependence then cancels out from the equation, as it should. On the other hand, Eq.(3) may also be recovered from Eq.(4), by postulating that for small X a singularity occurs when X approaches X_{crit} , namely

$$F(X) = \hat{f}(X - X_{crit})^{\beta_2}, \quad X - X_{crit} \ll 1, \quad (5)$$

with \hat{f} another non-universal amplitude. This phenomenological assumption implies a scaling relation for the shift of the critical value of the polymer reservoir packing fraction

$$X_{crit} = D^{1/\nu}t_\infty^{crit} \Rightarrow t_\infty^{crit} = X_{crit}D^{-1/\nu}. \quad (6)$$

Another scaling relation is implied for the critical amplitude $\hat{B}(D)$, namely

$$\hat{B}(D) = \hat{f}D^{(\beta_2 - \beta)/\nu}. \quad (7)$$

It is clear that the crossover between both power laws, Eq.(2) and Eq.(3), then also should occur when X is of

order unity, which implies very small values of t_∞ already when D is large. The region of $t_\infty - t_{\infty, \text{crit}}$ where Eq.(3) and Eq.(5) then hold is extremely small. Moreover, the general experience with problems of this kind is that a crossover never occurs abruptly [76, 82, 83, 84], but rather spans several decades of the corresponding crossover scaling variable ($X - X_{\text{crit}}$ in our case). In fact, if not a large enough range of this crossover scaling variable is accessible, one will instead observe a power law with “effective exponents” and “effective critical amplitudes”,

$$\Delta(D) \approx \hat{B}_{\text{eff}} t_D^{\beta_{\text{eff}}}, \quad (8)$$

where $\beta_2 < \beta_{\text{eff}} < \beta$ [50]. The effective exponents do not have a fundamental deep meaning, of course, since their values depend on the range of t_D that is used for the analysis in terms of Eq.(8), and hence are not really defined unambiguously.

III. MODEL AND SIMULATION METHOD

We consider a mixture of hard-sphere colloids with diameter σ_c and effective polymer spheres with diameter of gyration σ_p in the grand canonical ensemble. Throughout this work, the colloid diameter σ_c is taken to be the unit of length. In the grand canonical ensemble, the volume V and the respective fugacities, z_c and z_p , of colloids and polymers are fixed, while the number of particles in the system fluctuates. Following convention, the polymer fugacity is expressed in terms of a related quantity called the polymer reservoir packing fraction $\eta_p^r = \pi z_p \sigma_p^3 / 6$. We also introduce the colloid packing fraction $\eta_c = \pi \sigma_c^3 N_c / (6V)$, with N_c the number of colloids in the system. The particles interact via potentials that were originally proposed by Asakura and Oosawa [65] (AO) and later, independently, also by Vrij [66]. In this description, the so-called AO model, hard-sphere interactions are assumed between colloid-colloid and colloid-polymer pairs, while polymer-polymer pairs can interpenetrate freely. The interactions are thus strictly athermal such that the temperature plays no role. Instead, in the AO model, the analogue of (inverse) temperature is played by the polymer reservoir packing fraction η_p^r . As is well known, at the coexistence colloid fugacity and for sufficiently large colloid-to-polymer size ratios $q \equiv \sigma_p / \sigma_c$, the AO model exhibits a phase separation into a colloid-rich phase (the colloidal liquid) and colloid-poor phase (the colloidal vapor), provided η_p^r exceeds a critical value. Grand canonical Monte Carlo simulations are well suited to study this transition, and when combined with finite size scaling techniques these simulations also allow for investigations close to the critical point. Recently, this approach was applied to the bulk AO model, i.e. in the absence of walls, and the critical point was determined for $q = 0.8$, as well as the universality class, which was shown to be that of the 3D Ising model [67, 68].

In this work, grand canonical Monte Carlo simulations are used to study the AO model in confinement. To this end, we use a simulation box of dimensions $L_x \times L_y \times L_z$, with $L_x = L_y = L$ and $L_z = D$; the system volume thus equals $V = DL^2$. To capture the effect of confinement, we implement a so-called “sandwich” or “thin film” geometry. Here, periodic boundary conditions are applied in the x and y directions, while in the remaining z direction we place two parallel walls: one in the $z = 0$ plane, and in the $z = L_z$ plane. This closely resembles Ref. 46 where capillary condensation and evaporation of the AO model are investigated. Compared to the bulk AO model, one additional parameter is thus introduced, namely the film thickness D . For a film with thickness D , the thermodynamic limit is defined as the limit where the lateral dimensions $L_x = L_y = L$ of the film are taken to infinity. Throughout this work, the walls are taken to be hard, i.e. colloid-wall and polymer-wall overlaps are strictly forbidden. Note that this implies a strong attraction between the colloids and the walls due to the depletion effect [46]. The simulation method of Ref. 67 is then applied to the confined system; the main ingredients are a grand canonical cluster move [67] and a reweighting scheme [85].

IV. RESULTS

A. Binodal

For $q = 0.8$ and $D = 5$, the grand canonical distribution $P_L(\eta_c | \eta_p^r, z_c)$ is measured, defined as the probability of observing a system with colloid packing fraction η_c , at “inverse temperature” η_p^r and colloid fugacity z_c . There will generally be finite size effects in the lateral dimensions $L_x = L_y = L$ of the simulation box, denoted by the subscript L . Phase coexistence is established by tuning z_c such that $P_L(\eta_c | \eta_p^r, z_c)$ becomes bimodal with two peaks of equal area [86]. The respective packing fractions η_c^v and η_c^l , of the colloidal vapor and liquid phase, are obtained from the average peak positions. Typical distributions are shown in Fig. 1, plotted as $k_B T \ln P_L(\eta_c | \eta_p^r, z_c)$, with k_B the Boltzmann constant and T the temperature. In this way, the distributions correspond to *minus* the free energy of the system. The height F_L of the peaks in $k_B T \ln P_L(\eta_c | \eta_p^r, z_c)$, measured with respect to the minimum in between the peaks (arrow in Fig. 1), thus reflects the free energy barrier separating the colloidal vapor from the liquid phase [87]. In the two-phase region away from the critical point, the peaks in $P_L(\eta_c | \eta_p^r, z_c)$ are well separated and the barrier F_L will be large. Upon approach of the critical point, by lowering η_p^r , the peaks move closer together and the corresponding barrier F_L decreases profoundly.

To obtain the binodal, $P_L(\eta_c | \eta_p^r, z_c)$ is measured for a range of η_p^r and the average peak positions are recorded. The result is shown in Fig. 2. For comparison, the binodal of the bulk AO model is also shown, together with

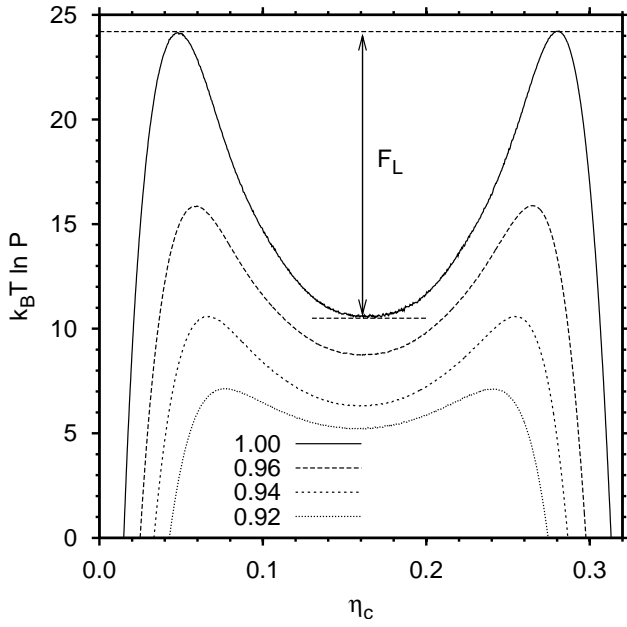


FIG. 1: Coexistence distributions of the confined AO model with colloid-to-polymer size ratio $q = 0.8$, lateral dimension $L = 15$, and film thickness $D = 5$ for several values of η_p^r as indicated. Note that we have plotted the *natural logarithm* of $P_L(\eta_c|\eta_p^r, z_c)$, multiplied by $k_B T$. In the above distributions, the colloid fugacity is tuned in order to obey the equal-weight prescription [86]. The barrier F_L in the distribution corresponding to $\eta_p^r = 1.0$ marks the average height of the peaks with respect to the minimum in between the peaks.

the bulk critical point taken from previous work [67, 68]. Note the familiar finite-size rounding in the simulation data close to the critical point (to describe the binodal correctly near the critical point requires finite size scaling, which we postpone to Fig. 10). The phase diagrams in Fig. 2 reveal the typical behavior of a fluid confined between two plates that undergoes a demixing transition: The critical point shows a significant shift which is accompanied by an inward shift of the binodal with respect to the bulk [18].

B. Cumulant analysis

To obtain the critical polymer reservoir packing fraction $\eta_{p,cr}^r$ of the confined system, the fourth order cumulant $U_4 = \langle m^2 \rangle^2 / \langle m^4 \rangle$ is measured, with $m = \eta_c - \langle \eta_c \rangle$, as function of η_p^r for various lateral dimensions L . The cumulant is obtained by taking appropriate moments of the distribution $P_L(\eta_c|\eta_p^r, z_c)$. For example, the average colloid packing fraction may be written as $\langle \eta_c \rangle(L, \eta_p^r, z_c) = \int_0^\infty \eta_c P_L(\eta_c|\eta_p^r, z_c) d\eta_c$, and similarly for the p -th order moment $\langle m^p \rangle(L, \eta_p^r, z_c) = \int_0^\infty [\eta_c - \langle \eta_c \rangle]^p P_L(\eta_c|\eta_p^r, z_c) d\eta_c$. Note that the outcome will generally depend on η_p^r , the colloid fugacity z_c , and the lateral system size L .

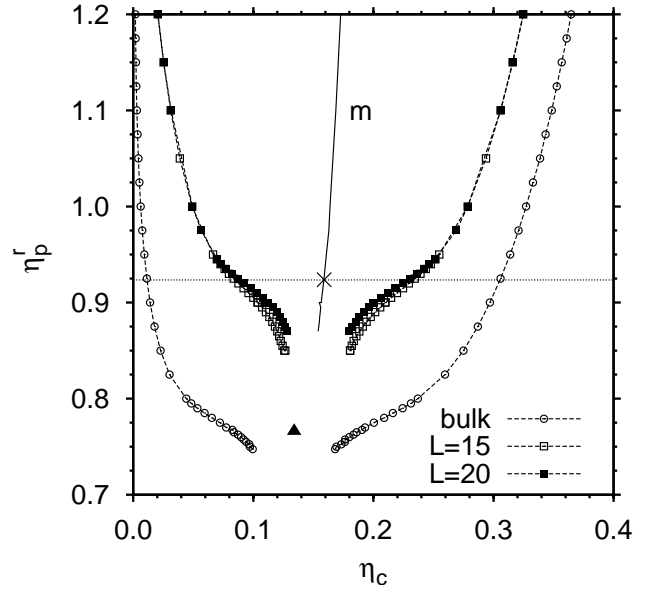


FIG. 2: Binodal of the AO model with $q = 0.8$ in bulk and confinement. Open circles show the bulk binodal, where the black triangle marks the corresponding critical point ($\eta_c = 0.134$; $\eta_p^r = 0.766$) obtained using finite size scaling [67, 68]. Open and closed squares show the binodal of the confined system with film thickness $D = 5$ for two lateral dimensions L . The horizontal line marks the critical polymer reservoir packing fraction $\eta_{p,cr}^r$ of the confined system in the limit $L \rightarrow \infty$ obtained using the cumulant intersection method, see Fig. 3. Lines connecting the points serve to guide the eye. Curve m shows the coexistence diameter $(\eta_c^l + \eta_c^v)/2$ of the confined system with $L = 20$.

Fig. 3 shows the cumulant as function of η_p^r for several system sizes L . We emphasize that the measurements were taken using the colloid fugacity at which the equal-weight prescription [86] was obeyed. At the critical point, the cumulant becomes system-size independent [88]. The intersections in Fig. 3 thus provide an estimate of the critical polymer reservoir packing fraction. We obtain $\eta_{p,cr}^r = 0.9238 \pm 0.0010$, where the error reflects the scatter in the various intersection points. This estimate is also shown in Fig. 2 (horizontal line). Defining the coexistence diameter as $(\eta_c^l + \eta_c^v)/2$ and ignoring finite size effects in this quantity for the moment, the intersection of the horizontal line with curve m (marked with a cross in Fig. 2) yields an estimate of the critical colloid packing fraction $\eta_{c,cr} \approx 0.159$. Compared to the bulk system, the critical colloid packing fraction has shifted to a slightly larger value.

The cumulant plot also provides evidence for the crossover scenario discussed in the introduction. From Fig. 3, we obtain $U_4 \approx 0.795$ at the critical point, which is between the 2D and 3D Ising values, see Table I. In the limit $L \rightarrow \infty$, U_4 is expected to approach the 2D Ising value. However, in the (still moderate) system sizes accessible in our simulations, “effective” critical behavior is observed instead, with properties between those of the

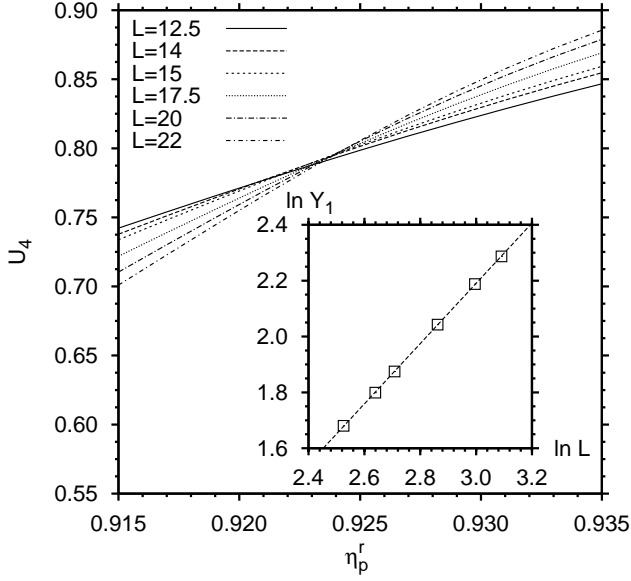


FIG. 3: Cumulant analysis of the confined AO model with $q = 0.8$ and film thickness $D = 5$. Shown is the fourth order cumulant U_4 as function of η_p^r for several lateral dimensions L . The intersection point yields an estimate of $\eta_{p,cr}^r$. The inset shows the cumulant slope Y_1 at the intersection point as function of the lateral dimension L .

2D and 3D Ising universality classes. Additional confirmation of the crossover may be obtained from an analysis of the cumulant slope $Y_1 \equiv dU_4/d\eta_p^r$ evaluated at the critical value of η_p^r . It is expected that $Y_1 \propto L^{1/\nu}$, with ν the critical exponent of the correlation length and L the lateral system size. To this end we have plotted, in the inset of Fig. 3, the cumulant slope Y_1 at the critical value $\eta_{p,cr}^r = 0.9238$ obtained above, versus the system size L . By performing a fit to the data, the exponent is measured to be $\nu_{eff} \approx 0.93$, which is already surprisingly close to the 2D Ising value. Obviously, ν_{eff} must be interpreted as an “effective” critical exponent.

TABLE I: Critical exponents of the order parameter (β), correlation length (ν), and specific heat (α) for the two-dimensional (2D) and three-dimensional (3D) Ising model, as well as the mean-field values (MF). Also listed is the value of the fourth order cumulant (U_4) at criticality for the 2D and 3D Ising model.

	β	ν	α	U_4
2D	1/8	1	0	0.856 [89]
3D	0.326 [90]	0.630 [90]	0.109 [90]	0.629 ^a
MF	1/2	1/2	0	—

^aobtained from the 3D Ising universal fixed point distribution of Ref. 91.

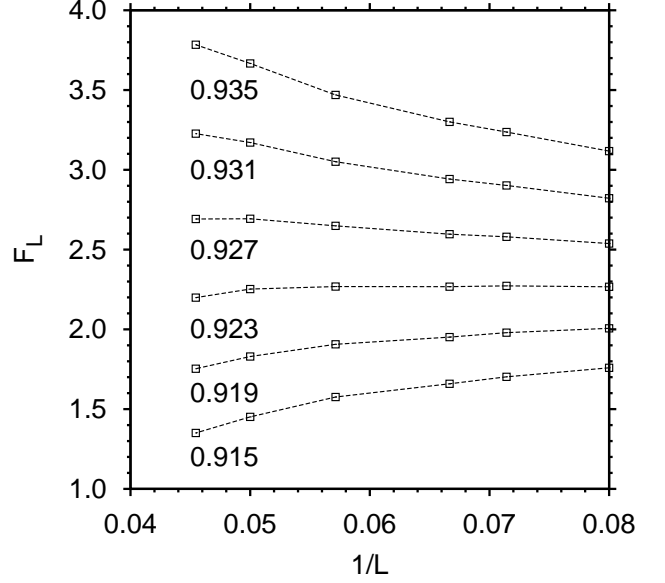


FIG. 4: Finite size dependence of the free energy barrier F_L between the colloidal vapor and liquid phase, for the confined AO model with $q = 0.8$ and film thickness $D = 5$. Shown is F_L as function of $1/L$ at the indicated value of η_p^r , with L the lateral dimension of the simulation box. The barrier was extracted from equal-area [86] distributions $P_L(\eta_c|\eta_p^r, z_c)$, see also Fig. 1.

C. Free energy barrier and interfacial tension

Next, we consider the free energy barrier F_L between the colloidal vapor and liquid phase. At the critical point, the grand canonical distribution scales with the system size L as [88, 92]

$$P_L^*(\eta_c) = b_0 L^{\beta/\nu} \mathcal{P}^0(b_0 L^{\beta/\nu} \eta_c), \quad (9)$$

where $P_L^*(\eta_c)$ is the distribution $P_L(\eta_c|\eta_p^r, z_c)$ measured in the finite system at the critical values of η_p^r and z_c , b_0 some non-universal constant, and \mathcal{P}^0 a function independent of system size (in the present case of confinement, the critical exponents β and ν assume 2D Ising values). Recall from Fig. 1 that F_L is given by the peak-to-valley height in the logarithm of $P_L(\eta_c|\eta_p^r, z_c)$. The scaling form of Eq.(9) thus implies that F_L becomes system-size independent at the critical point, providing an alternative route to locate $\eta_{p,cr}^r$ (see Ref. 93 where this approach is applied to the Lennard-Jones fluid). To locate $\eta_{p,cr}^r$, the barrier is recorded as function of L for several values of η_p^r . At the critical value of η_p^r , a plateau should be visible. For the confined AO model, the latter is verified in Fig. 4, which shows F_L as function of $1/L$ for various η_p^r around the critical region. The figure shows an increase in F_L with system size at high η_p^r , and a decrease at low η_p^r . The plateau occurs in the interval $\eta_p^r = 0.923 - 0.927$. Although not very precise, this estimate is consistent with the previous result based on the intersection of the cumulant.

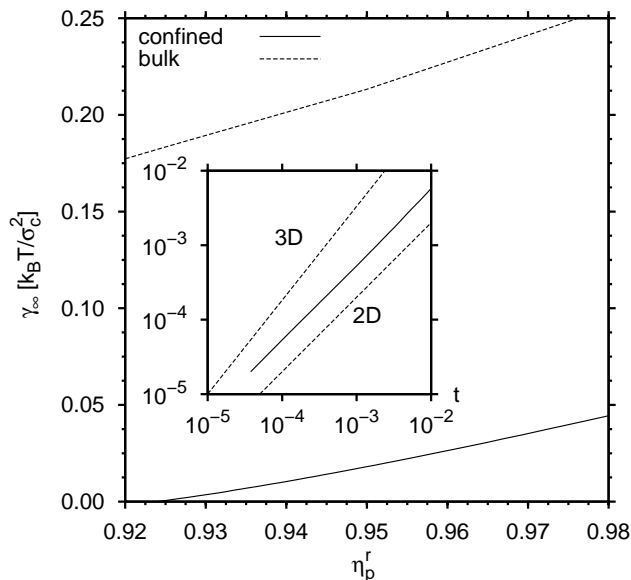


FIG. 5: *main frame*: Interfacial tension γ_∞ of the confined AO model with $q = 0.8$ and $D = 5$ as function of η_p^r (solid curve), as well as the corresponding bulk interfacial tension (dashed curve). *inset*: γ_∞ of the confined system as function of the relative distance from the critical point t , on double logarithmic scales, where $\eta_{p,cr}^r = 0.9241$ in t was used. The dashed lines illustrate 2D and 3D Ising exponents.

A more precise estimate of $\eta_{p,cr}^r$ may be obtained from the critical behavior of the interfacial tension γ_∞ in the thermodynamic limit. Upon approach of the critical point, starting in the two-phase region, the interfacial tension is expected to vanish as [76]

$$\gamma_\infty = \Gamma_0 t^\mu, \quad \mu = 2 - \alpha - \nu, \quad (10)$$

with $t = \eta_p^r / \eta_{p,cr}^r - 1$ the relative distance from the critical point, critical amplitude Γ_0 , and critical exponents listed in Table I. For 2D Ising systems we thus obtain $\mu_{2D} = 1$ and for 3D Ising systems $\mu_{3D} = 2\nu$, where in the latter the hyperscaling relation $2 - \alpha = d\nu$ was used (with d the spatial dimension). For 3D bulk, the expected exponent 2ν was already confirmed by us in Ref. 68. In the present case of confinement, however, the crossover scaling scenario implies a transition in the critical behavior of γ_∞ from singular ($\mu = 2\nu$) in three dimensions to purely regular ($\mu = 1$) in two dimensions. This particularly affects the *slope* of γ_∞ versus t at the critical point, which should be zero in 3D, and finite positive in 2D.

In order to test if evidence for this change in critical behavior is present in our simulation data, we use the free energy barrier F_L to measure the interfacial tension. Following Ref. 87, the interfacial tension γ_L in a confined system of thickness D and finite lateral dimension $L \gg D$ equals $\gamma_L = F_L / (2LD)$, where the factor of two stems from the use of periodic boundary conditions. The thermodynamic limit $L \rightarrow \infty$ can be evaluated through an elimination of finite size effects using the extrapolation

equation [87]

$$\gamma_L = \gamma_\infty + \frac{a_1}{LD} + \frac{a_2 \ln(L)}{LD}, \quad (11)$$

where the constants a_1 and a_2 are *a priori* unknown. The interfacial tension in the thermodynamic limit $\gamma_\infty(\eta_p^r)$ at a given value of η_p^r may thus be obtained by fitting Eq.(11) to corresponding measurements of $\gamma_L(\eta_p^r)$ in finite systems. We have applied this approach using different system sizes between $L = 12.5 - 22$ and furthermore assuming $a_2 = 0$ in Eq.(11). The latter choice is based on empirical findings that the logarithmic term in Eq.(11) is typically rather weak, at least for Ising-like systems [68, 94]. The result is summarized in Fig. 5. The main frame shows the thermodynamic limit interfacial tension γ_∞ as function of η_p^r for the confined AO model, as well as the bulk tension taken from previous work [68]. Note the pronounced *decrease* in the interfacial tension of the confined system with respect to the bulk, a direct consequence of the upward shift in $\eta_{p,cr}^r$. For the confined system, the vanishing of γ_∞ at the critical point yields $\eta_{p,cr}^r = 0.9241$ which is consistent with our previous estimate based on the intersection of the cumulant. Moreover, the interfacial tension seems to vanish with finite slope, a point further emphasized in the inset where γ_∞ is plotted as function of the relative distance from the critical point. Note that the interfacial tension in the confined system is already well described by the 2D Ising exponent.

D. Order parameter

Another consequence of the crossover scenario is that the binodal should appear “flatter”, since the critical exponent β of the order parameter for the 2D Ising model is smaller than in 3D. In this section, we use the finite size scaling algorithm of Kim, Fisher, and Luijten [95] to study the critical behavior of the order parameter in confinement. The algorithm is based on the dependence of the cumulant U_4 on the temperature-like variable η_p^r , the colloid fugacity z_c , and the system size L (recall that U_4 is defined in Section IV B). For fixed η_p^r and L , it is straightforward to measure U_4 and $\langle \eta_c \rangle$ as function of z_c . A plot of U_4 versus $\langle \eta_c \rangle$, which is thus parameterized by z_c , reveals two minima separated by a maximum, see Fig. 6. The location of the minimum at low colloid packing fraction is denoted $\eta_c^-(L, \eta_p^r)$, with $Q^-(L, \eta_p^r)$ the corresponding minimum value. Similarly, the location of the minimum at high colloid packing fraction is denoted $\eta_c^+(L, \eta_p^r)$, with $Q^+(L, \eta_p^r)$ the corresponding minimum value. Note that the location of the minima, and the corresponding minimum values, depend on η_p^r and L , but obviously not on z_c . In the thermodynamic limit $L \rightarrow \infty$, U_4 approaches $1/3$ in the one-phase region (horizontal dashed lines in Fig. 6). On the phase-boundary, $\eta_c^-(L, \eta_p^r)$ and $\eta_c^+(L, \eta_p^r)$ approach the thermodynamic values $\eta_c^-(\eta_p^r)$ and $\eta_c^+(\eta_p^r)$, respectively, while $Q^-(L, \eta_p^r)$

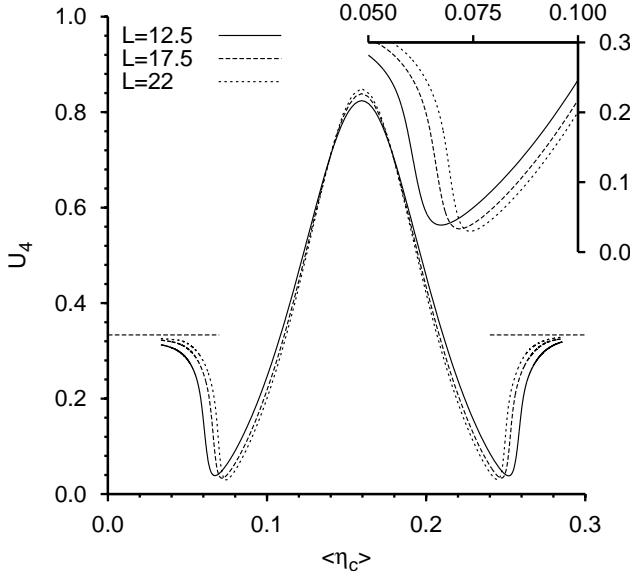


FIG. 6: Cumulant ratio U_4 as function of the average colloid packing fraction $\langle \eta_c \rangle$. The data were obtained for the confined AO model with $q = 0.8$ at $\eta_p^r = 0.93$, film thickness $D = 5$, and several lateral dimensions L as indicated. Dashed horizontal lines correspond to the limiting value $U_4 = 1/3$, see details in text. The inset shows the region around $\eta_c^-(L, \eta_p^r)$ on an expanded scale.

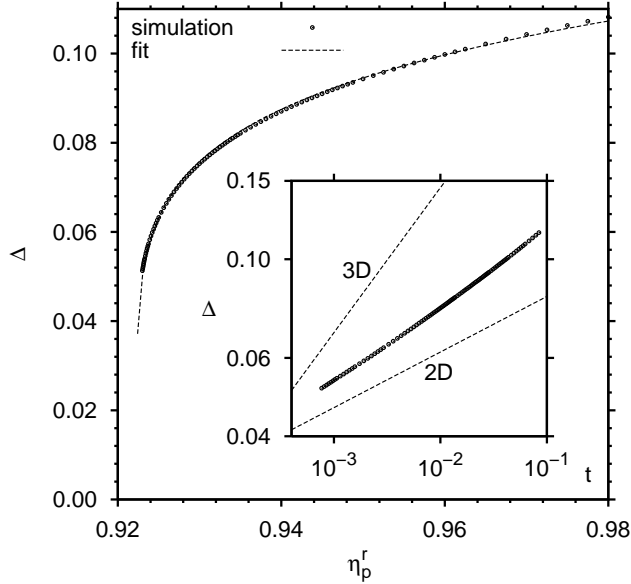


FIG. 7: Order parameter Δ as function of η_p^r for the confined AO model with $q = 0.8$ and film thickness $D = 5$. The main frame shows Δ in the thermodynamic limit as function of η_p^r on linear scales, where the curve through the simulation data is a fit to Eq.(8). The inset shows the result as function of the relative distance from the critical point $t = \eta_p^r / \eta_{p,cr}^r - 1$, on double logarithmic scales, where the slopes of the lines reflect 2D and 3D Ising critical exponents.

and $Q^+(L, \eta_p^r)$ approach zero [96]. The L -dependence shown in Fig. 6 is consistent with this scenario, see also the inset.

In order for the scaling algorithm to succeed, simulation data for at least three different system sizes are required. In this work, $L = 15, 17.5$ and 20 are used. In addition, measurements over a rather broad range in η_p^r are required, starting in the two-phase region and stretching toward the critical point. Here, five different η_p^r are simulated per system size, evenly distributed over the range $\eta_p^r \approx 0.9 - 1.0$. Estimates of properties at intermediate η_p^r are obtained using histogram extrapolation [97]. The purpose of the scaling algorithm is to evaluate the order parameter Δ as function of η_p^r in the thermodynamic limit

$$\Delta(\eta_p^r) = \lim_{L \rightarrow \infty} \frac{\eta_c^+(L, \eta_p^r) - \eta_c^-(L, \eta_p^r)}{2}. \quad (12)$$

Following Ref. 95, we define the quantities

$$Q_{\min}(L, \eta_p^r) \equiv \frac{Q^+(L, \eta_p^r) + Q^-(L, \eta_p^r)}{2}, \quad (13)$$

$$x(L, \eta_p^r) \equiv Q_{\min}(L, \eta_p^r) \ln \left[\frac{4}{e Q_{\min}(L, \eta_p^r)} \right], \quad (14)$$

$$y(L, \eta_p^r) \equiv \frac{\eta_c^+(L, \eta_p^r) - \eta_c^-(L, \eta_p^r)}{2 \Delta(\eta_p^r)}. \quad (15)$$

The algorithm starts in the two-phase region, with a value of η_p^r significantly above its critical value. The peaks in $P_L(\eta_c | \eta_p^r, z_c)$ are then well separated and the free energy barrier F_L will be large (see for example the distribution corresponding to $\eta_p^r = 1.0$ in Fig. 1). This regime is called the “gaussian limit” because $P_L(\eta_c | \eta_p^r, z_c)$ may be described by a sum of two gaussians in this case [95]. In the gaussian limit, it can be shown rigorously that the points (x, y) of different system sizes L , should all collapse onto the line $y = 1 + x/2$. Recall that $\Delta(\eta_p^r)$ in Eq.(15) is the order parameter in the thermodynamic limit at the considered η_p^r , precisely the quantity of interest, which may thus be obtained by fitting until the best collapse onto $y = 1 + x/2$ occurs. Next, η_p^r is chosen closer to the critical point, the points (x, y) are calculated as before, but this time around $\Delta(\eta_p^r)$ is chosen such that the new data set joins smoothly with the previous one, yielding an estimate of the order parameter at the new η_p^r . This procedure is repeated as closely as possible to the critical point, where Δ vanishes, yielding an estimate of $\eta_{p,cr}^r$.

For the confined AO model, the output of the scaling algorithm is illustrated in Fig. 7. The main frame shows the order parameter as function of η_p^r on linear scales. The dashed curve is a fit to the simulation data using Eq.(8) from which $\eta_{p,cr}^r = 0.9223$, $\hat{B}_{\text{eff}} = 0.173$, and $\beta_{\text{eff}} = 0.17$ are obtained. As before, β_{eff} plays the role of an effective critical exponent. Note that β_{eff} is already rather close to the pure 2D Ising value. This point is emphasized in the inset of Fig. 7, which shows the order

parameter as function of the relative distance from the critical point t , where $\eta_{p,cr}^r = 0.9223$ in t was used. Also included are power laws illustrating 2D and 3D Ising critical exponents. As expected, the simulation data slowly approach the slope of the 2D Ising exponent. By performing additional simulations using larger lateral dimensions L , the data can in principle be extended to smaller values of t , where the pure 2D Ising exponent will become visible. However, such simulations are computationally very demanding and beyond the scope of the present investigation. In contrast, adding data at larger values of t in order to observe the 3D Ising exponent is not possible, since then we leave the critical regime. In hindsight, the thickness $D = 5$ considered here is too small to observe the full crossover from 3D to 2D Ising critical behavior. For such thin films, the critical behavior is essentially 2D Ising. The crossover scaling is expected to be visible only in much thicker films, where 2D Ising behavior shows up at extremely small t .

In addition to the order parameter, the scaling algorithm also yields y as function of x . The latter function, or scaling curve, is significant because it is universal within a universality class. For bulk 3D fluids, belonging to the 3D Ising universality class, universality of the scaling curve has been verified for the hard-core square-well (HCSW) fluid [95], the restricted primitive model (RPM) [95], the decorated lattice gas [95], the AO model [98], and the Widom-Rowlinson mixture [99]. In the present case of confinement, however, the scaling curve is expected to deviate profoundly from the bulk 3D Ising form. The latter is verified in Fig. 8, which shows the scaling curve of the confined AO model obtained in this work, together with the scaling curve of the 3D bulk HCSW fluid [95]. Following the convention of Ref. 95, the scaling curve has been raised to an exponent $-\phi = -1/\beta$, with $\beta = 1/8$ the critical exponent of the 2D Ising model. An important feature of Fig. 8 is that, for small x , the data of the confined AO model correctly approach the limiting form $y = 1 + x/2$. In addition, we observe that the data from the three different system sizes have collapsed accurately onto a single curve. As expected, the scaling curve of the 3D bulk HCSW fluid differs profoundly from the one of the confined AO model, a direct consequence of the different universality classes. Note in particular the large difference in x_c at which the scaling curve vanishes. For the HCSW fluid, $x_c \approx 0.286$ [95], which exceeds the value of the confined AO model $x_c \approx 0.165$ by over 60%. For the 2D Ising model, $x_c \approx 0.46$ is reported [95], which overestimates our value significantly. Note, however, that the scaling curve of Fig. 8 must be regarded as an “effective” scaling curve, and that deviations from the pure 2D Ising form are to be expected.

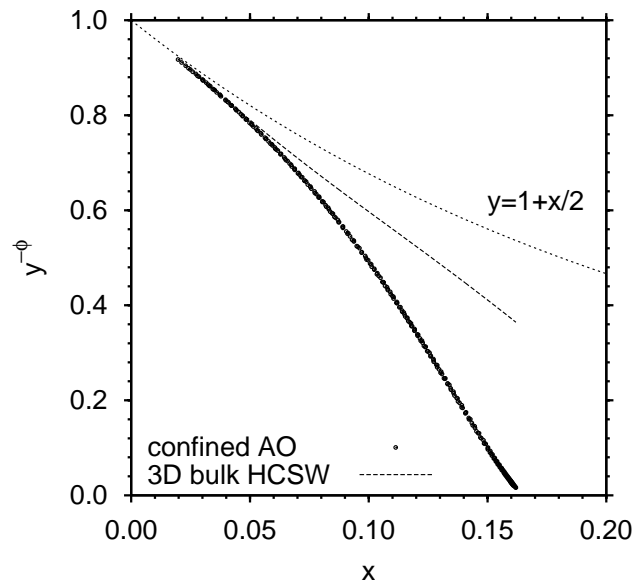


FIG. 8: Order parameter scaling curve $y^{-\phi}$, with $\phi = 1/\beta$ and $\beta = 1/8$, for both the 3D bulk HCSW fluid [95], and the confined AO model ($q = 0.8$ and $D = 5$) of this work. Also shown is the exact small x form $y = 1 + x/2$ of the gaussian limit.

E. Coexistence diameter

Finally, we turn to the critical behavior of the coexistence diameter $\delta \equiv (\eta_c^l + \eta_c^v)/2$, in general given by [100]

$$\delta = \eta_{c,cr} (1 + A_{2\beta} t^{2\beta} + A_{1-\alpha} t^{1-\alpha} + A_1 t), \quad (16)$$

with $\eta_{c,cr}$ the colloid packing fraction at the critical point, t the relative distance from the critical point, and non-universal amplitudes A_i . The term proportional to $t^{2\beta}$ is due to pressure mixing, and for systems where pressure mixing is absent $A_{2\beta} = 0$. It is not yet clear which features determine the degree of pressure mixing in a fluid. Of the bulk 3D fluids where this issue has been investigated, only the RPM exhibits substantial pressure mixing [95]. In the decorated lattice gas, pressure mixing is absent [95], and the same seems to be the case for the Widom-Rowlinson mixture [99]. Simulations of the HCSW fluid [95] and the AO model [98] point to rather weak pressure mixing.

To obtain the coexistence diameter of a bulk 3D fluid is still challenging. In the present case of confinement the situation is even more subtle. Assuming negligible pressure mixing, the critical behavior of the diameter is dominated by $t^{1-\alpha}$. The crossover scaling scenario then implies a transition from weak singular behavior $\alpha \approx 0.109$ in 3D, to purely regular behavior $\alpha = 0$ in 2D, see Table I. On the other hand, if pressure mixing is important, the diameter remains singular and dominated by $t^{2\beta}$, with ultimately $\beta = \beta_2$ the critical order parameter exponent of the 2D Ising model. To determine which of these scenar-

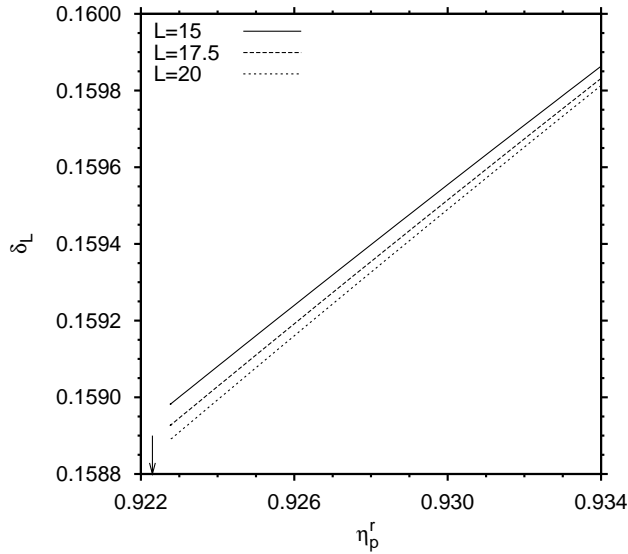


FIG. 9: Coexistence diameter δ_L given by Eq.(18) of the confined AO model with $q = 0.8$ and $D = 5$ obtained in finite systems of lateral dimension L as indicated. The arrow marks the estimate $\eta_{p,cr}^r \approx 0.9223$ obtained from Fig. 7.

ios is realized in the confined AO model, we again use the finite size scaling approach of Kim, Fisher, and Luijten [95]. Note that, in addition to the order parameter, these authors also present an algorithm to extract the diameter. As before, the algorithm generates a scaling curve, starting with data obtained well away from the critical point, and then recursively working its way down toward criticality. However, the quantities needed to construct the scaling curve are different. In particular, they involve the asymmetry factor

$$A_{\min}(L, \eta_p^r) \equiv \frac{Q^+(L, \eta_p^r) - Q^-(L, \eta_p^r)}{Q^+(L, \eta_p^r) + Q^-(L, \eta_p^r)}, \quad (17)$$

with $Q^\pm(L, \eta_p^r)$ defined previously. Unfortunately, for the confined AO model, we were unable to extract the diameter in this way. Closer inspection of our data revealed that A_{\min} as function of η_p^r changes sign from negative to positive upon approach of the critical point, and this makes the procedure numerically unstable. In contrast, for 3D bulk systems, A_{\min} remains positive (at least for the AO model and the Widom-Rowlinson mixture) and so the problem does not occur there.

Hence, our attempt to extract the critical behavior of the diameter in confinement is unsuccessful. Instead, we follow the more pragmatic approach of Ref. 101 and simply show in Fig. 9 the diameter of the finite system

$$\delta_L(\eta_p^r) \equiv \frac{\eta_c^+(L, \eta_p^r) + \eta_c^-(L, \eta_p^r)}{2}, \quad (18)$$

with $\eta_c^\pm(L, \eta_p^r)$ defined as before. Obviously, these data cannot be used to extract (effective) critical exponents, but the value $\eta_{c,cr} \approx 0.159$ of Section IV B derived from equal-area distributions $P_L(\eta_c | \eta_p^r, z_c)$ seems confirmed.

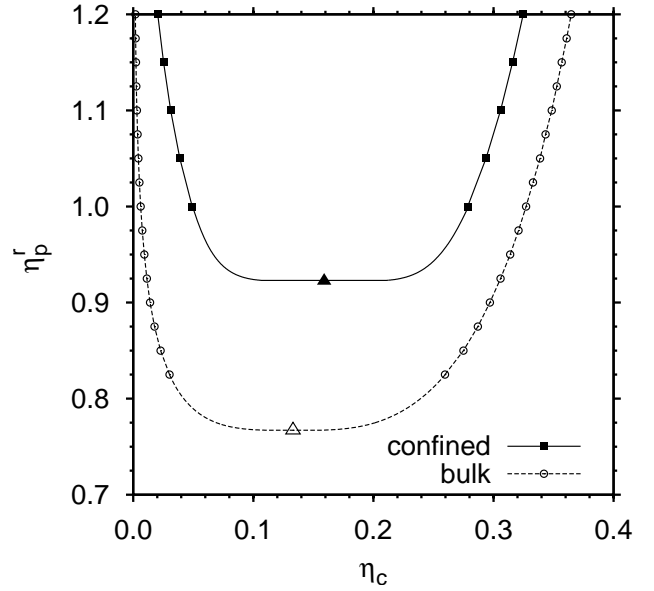


FIG. 10: Thermodynamic limit binodals, obtained using finite size scaling, of the AO model with $q = 0.8$ in bulk and confinement. The dashed curve shows the bulk binodal, the solid curve is the binodal in the confined system with thickness $D = 5$. Triangles mark the corresponding critical points; squares and circles are raw simulation data obtained in finite systems away from the critical point.

V. DISCUSSION AND CONCLUSION

In this work, we have investigated the critical behavior of a colloid-polymer mixture confined to a thin film of thickness $D = 5$. The main finding is that for such thin films, 2D Ising universality is clearly visible. The latter is manifested by the critical exponents of the correlation length, the interfacial tension, and the order parameter. Since the order parameter exponent in 2D Ising systems is smaller than in 3D, the binodal in the confined system should appear “flatter”. To emphasize this point, we have combined the order parameter data of Fig. 7 with the coexistence diameter of the largest system in Fig. 9, and constructed the binodal in the thermodynamic limit. The result is shown in Fig. 10 as the solid curve, where the closed triangle marks the location of the critical point. As expected, away from the critical point, the binodal obtained via finite size scaling joins smoothly with the raw finite-size simulation data (squares). For comparison, the binodal of the bulk system in the thermodynamic limit is also shown, taken from previous work [68]. The different curvature of the binodals should be detectable in experiments. The result of Fig. 10 may furthermore be relevant to Gibbs ensemble simulations of fluids in confined geometry. Here, the critical point is typically determined via a fitting procedure assuming 3D Ising exponents. In contrast, Fig. 10 indicates that for thin films, extrapolations using 2D Ising exponents may be more appropriate.

In addition to a flatter binodal, the location of the critical point also changes with respect to the bulk. Our results indicate a pronounced shift of the critical point toward higher values of η_p^r , as well as a slight increase in the critical colloid packing fraction $\eta_{c,cr}$. The increase in η_p^r is consistent with previous work on capillary condensation in the AO model that was based on DFT and Gibbs ensemble simulations [46]. The behavior of $\eta_{c,cr}$ is more subtle. For films with $D \geq 5\sigma_c$, DFT shows an *increase* in $\eta_{c,cr}$ with respect to the bulk value, while for very thin films a *decrease* is predicted [46]. It is not obvious if the corresponding Gibbs ensemble simulations also follow this trend [46]. At first sight, the increase in $\eta_{c,cr}$ observed in our simulations seems consistent with the trend predicted by DFT for films with $D \geq 5\sigma_c$. However, for very thick films, $\eta_{c,cr}$ must ultimately approach its bulk value again, and it is not clear how the DFT of Ref. 46 approaches this limit. Interestingly, recent Gibbs ensemble simulations of the confined Lennard-Jones fluid with film thickness $D = 12$ particle diameters, show a pronounced *decrease* in the critical density [101], which differs from both the present simulation result, and the DFT trend for this rather thick film.

All in all, the critical density seems to depend quite sensitively on the details of the particle and wall interactions, as well as on the film thickness. Key to a reliable estimate of the critical density is a precise description of the coexistence diameter. The latter may be obtained using the finite size scaling approach of Ref. 95, as was recently demonstrated for 3D bulk fluids [95, 98, 99]. The issues pertaining to the shift of the critical density in con-

finement inspired us, in Section IV E, to apply this scaling algorithm to the confined AO model. Unfortunately, we were unable to extract the diameter because the scaling algorithm of Ref. 95 seems to behave profoundly different in confinement; the source is a numerical instability arising from a change in sign of the asymmetry factor given by Eq.(17). At this point, we see no reliable way to extract the coexistence diameter of the confined AO model; nor do we understand the significance of the change in sign in A_{\min} . To resolve these issues would be the subject of further work.

Regarding the order parameter, no difficulties were encountered in applying Ref. 95 to the confined AO model. This was demonstrated by the accurate collapse of the data from different system sizes onto a single scaling curve. Also the estimated effective critical exponent β_{eff} is consistent with the crossover scaling scenario. Nevertheless, the large discrepancy in x_c at which the scaling curve vanishes, between the confined AO model and the 2D Ising model, is concerning. To understand the source of this discrepancy, too, would require further work.

Acknowledgments

We are grateful to the *Deutsche Forschungsgemeinschaft* (DFG) for support (TR6/A5 and TR6/D3). JH also acknowledges support of the DFG under Grants No. HO 2231/2-1 and HO 2231/2-2.

-
- [1] G. Decker and J. B. Schlenoff (eds.), *Multilayer Thin Films: Sequential Assembly of Nanocomposite Materials* (Wiley-VCH, Weinheim, 2002)
 - [2] E. L. Wolf, *Nanophysics and Nanotechnology* (Wiley-VCH, Weinheim, 2004)
 - [3] Y. Champion and H. J. Fecht (eds.), *Nano-Architected and Nano-Structured Materials* (Wiley-VCH, Weinheim, 2004)
 - [4] C. N. R. Rao, A. Müller, and A. K. Cheetham (eds.) *The Chemistry of Nanomaterials* (Wiley VCH, Weinheim, 2004)
 - [5] R. Kelsall, I.W. Hamley and M. Geoghegan (eds.), *Nanoscale Science and Technology* (Wiley-VCH, Weinheim, 2005)
 - [6] L. D. Gelb, K. E. Gubbins, R. Radhakrishnan, and M. Sliwinska-Bartkowiak, Rep. Progr. Phys. **62**, 1573 (1999)
 - [7] H. Watarai, *Interfacial Nanochemistry: Molecular Science and Engineering at Liquid-Liquid Interfaces* (Springer, Berlin, 2005)
 - [8] S. J. Gregg and K. S. W. Sing, *Adsorption, Surface Area, and Porosity*, 2nd Ed. (Academic Press, New York, 1982)
 - [9] A. J. Liapis (ed.) *Fundamentals of Adsorption* (Engineering Foundation, New York, 1987)
 - [10] F. Rouquerol, J. Rouquerol, and K. S. W. Sing, *Adsorption by Powders and Porous Solids: Principles, Methodology, and Applications* (Academic Press, San Diego, 1999)
 - [11] J. S. Rowlinson and B. Widom, *Molecular Theory of Capillarity* (Oxford Univ. Press, London, 1982)
 - [12] C. A. Croxton (ed.) *Fluid Interfacial Phenomena* (Wiley, New York, 1985)
 - [13] J. Charvolin, J.-F. Joanny, and J. Zinn-Justin (eds.) *Liquids at Interfaces* (North-Holland, Amsterdam, 1990)
 - [14] D. Henderson (ed.) *Fundamentals of Inhomogeneous Fluids* (M. Dekker, New York, 1992)
 - [15] K. Binder, D. Landau, and M. Müller, J. Stat. Phys. **110**, 1411 (2003)
 - [16] W. T. Thomson (Lord Kelvin), Philos. Mag. **42**, 448 (1871)
 - [17] D. Nicholson, J. Chem. Soc. Faraday Trans. I. **71**, 238 (1975); *ibid* **72**, 29 (1976)
 - [18] M. E. Fisher and H. Nakanishi, J. Chem. Phys. **75**, 5857 (1981); H. Nakanishi and M.E. Fisher, J. Chem. Phys. **78**, 3279 (1983)
 - [19] R. Evans and P. Tarazona, Phys. Rev. Lett. **52**, 557 (1987); R. Evans and U. M. B. Marconi, Chem. Phys. Lett. **114**, 415 (1985); R. Evans, U. M. B. Marconi and P. Tarazona, J. Chem. Soc. Faraday Trans II **82**, 1763 (1986)

- [20] B. K. Peterson, J. P. R. B. Walton, and K. E. Gubbins, *J. Chem. Soc. Faraday Trans. II* **82**, 1789 (1986); B. K. Peterson, K. E. Gubbins, G. S. Heffelfinger, U. M. B. Marconi, and F. van Swol, *J. Chem. Phys.* **88**, 6487 (1988)
- [21] R. Evans, *J. Phys.: Condens. Matter* **2**, 8989 (1990)
- [22] A. O. Parry and R. Evans, *J. Phys. A: Math. Gen.* **25**, 275 (1992)
- [23] E. Carlon, A. Drzewinski, and J. Rogiers, *Phys. Rev. B* **58**, 5078 (1998); E. Carlon and K. Szota, preprint (2005) "Correction to the Kelvin equation for long-range boundary fields".
- [24] C. Varea and A. Robledo, *Physica A* **268**, 391 (1999)
- [25] K. G. Kornev, I. K. Shingareva, and A. V. Neimark, *Adv. Colloid Interface Sci.* **96**, 143 (2002)
- [26] B. K. Peterson, J. P. R. B. Walton and K. E. Gubbins, *Int. J. Thermophys.* **6**, 585 (1985); G. S. Heffelfinger, F. van Swol, and K. E. Gubbins, *Mol. Phys.* **61**, 1381 (1987); *J. Chem. Phys.* **88**, 6487 (1988)
- [27] A. Z. Panagiotopoulos, *Mol. Phys.* **62**, 701 (1987)
- [28] U. Heinbuch and J. Fischer, *Chem. Phys. Lett.* **135**, 587 (1987); S. Sokolowski and J. Fischer, *Molec. Phys.* **71**, 393 (1990)
- [29] M. Schoen, J. H. Cushman, D. J. Diestler, and C. L. Rhykerd, *J. Chem. Phys.* **88**, 1394 (1988)
- [30] J. M. D. MacElroy and S.-H. Suh, *Molecular Simul.* **2**, 313 (1989)
- [31] J. P. R. B. Walton and N. Quirke, *Molecular Simul.* **2**, 361 (1989)
- [32] D. Nicolaidis and R. Evans, *Phys. Rev. B* **39**, 9336 (1989)
- [33] E. V. Albano, K. Binder, D. W. Heermann, and W. Paul, *J. Chem. Phys.* **91**, 3700 (1989); E. V. Albano, K. Binder, and W. Paul, *J. Phys.: Condens. Matter* **12**, 2701 (2000)
- [34] K. Binder and D. P. Landau, *J. Chem. Phys.* **96**, 1444 (1992)
- [35] O. Dillmann, W. Janke, M. Müller, and K. Binder, *J. Chem. Phys.* **114**, 5853 (2001)
- [36] E. Kierlik, Y. Fan, P. A. Monson, and M. L. Rosenberg, *J. Chem. Phys.* **102**, 3712 (1994)
- [37] W. T. Gózdź, K. E. Gubbins, and A. Z. Panagiotopoulos, *Mol. Phys.* **84**, 825 (1995); W. T. Gózdź, *J. Chem. Phys.* **122**, 074505 (2005)
- [38] J. E. Curry and J. H. Cushman, *Mol. Phys.* **85**, 173 (1995); *J. Chem. Phys.* **103**, 2132 (1995)
- [39] T. Flebbe, B. Dünweg, and K. Binder, *J. Phys. (Paris) II* **6**, 665 (1996)
- [40] M. Müller and K. Binder, *Macromolecules* **31**, 8323 (1998)
- [41] N. B. Wilding, F. Schmid, and P. Nielaba, *Phys. Rev. E* **58**, 2201 (1998)
- [42] K. Grabowski, A. Patrykiewicz, and S. Sokolowski, *Thin Solid Films* **379**, 297 (2000)
- [43] O. Pizio, A. Patrykiewicz, and S. Sokolowski, *Mol. Phys.* **99**, 57 (2001)
- [44] H. Bock, D. J. Diestler, and M. Schoen, *J. Phys.: Condens. Matter* **13**, 4697 (2001)
- [45] D. Woywod and M. Schoen, *Phys. Rev. E* **67**, 026122 (2003)
- [46] M. Schmidt, A. Fortini, and M. Dijkstra, *J. Phys.: Condens. Matter* **15**, S3411 (2003); M. Schmidt, A. Fortini, and M. Dijkstra, *J. Phys.: Condens. Matter* **16**, S4159 (2004)
- [47] M. Müller and K. Binder, *J. Phys.: Condens. Matter* **17**, S333 (2005)
- [48] K. Binder, *Thin Solid Films* **20**, 367 (1974)
- [49] F. Freire, D. O'Connor and C. R. Stephens, *J. Stat. Phys.* **74**, 219 (1994)
- [50] Y. Rouault, J. Baschnagel and K. Binder, *J. Stat. Phys.* **80**, 1009 (1995)
- [51] H. Dominguez, M. P. Allen, and R. Evans, *Mol. Phys.* **96**, 209 (1999)
- [52] S. Varga, D. Boda, D. Henderson and S. Sokolowski, *J. Colloid Interface Sci.* **227**, 223 (2000)
- [53] P. Bryk, L. Lajtan, O. Pizio, Z. Sokolowska and S. Sokolowski, *J. Colloid Interface Sci.* **229**, 526 (2000)
- [54] M. E. Fisher, *Rev. Mod. Phys.* **46**, 587 (1974)
- [55] R. van Roij, M. Dijkstra, and R. Evans, *Europhys. Lett.* **49**, 350 (2000); R. van Roij, M. Dijkstra, and R. Evans, *J. Chem. Phys.* **113**, 7689 (2000); M. Dijkstra, R. van Roij, and R. Evans, *Phys. Rev. E* **63**, 051703 (2001)
- [56] A. Patrykiewicz, S. Sokolowski, and K. Binder, *Surface Sci. Repts.* **37**, 207 (2000)
- [57] L. Salamacha, A. Patrykiewicz, S. Sokolowski, and K. Binder, *J. Chem. Phys.* **122**, 074703 (2005)
- [58] W. C. K. Poon and P. N. Pusey, in *Observation, Prediction and Simulation of Phase Transitions in Complex Fluids*, edited by M. Baus, L. F. Rull, and J. P. Ryckaert) p. 3 (Kluwer Acad. Publ., Dordrecht, 1995)
- [59] A. K. Arora and B. V. R. Tata, *Adv. Colloid Interface Sci.* **78**, 49 (1998)
- [60] H. Löwen, *J. Phys.: Condens. Matter* **13**, R 415 (2001)
- [61] W. Poon, *J. Phys.: Condens. Matter* **14**, R 589 (2002)
- [62] D. G. A. L. Aarts, J. H. van der Wiel, and H. N. W. Lekkerkerker, *J. Phys.: Condens. Matter* **15**, S245 (2003)
- [63] D. G. A. L. Aarts, M. Schmidt, and H. N. W. Lekkerkerker, *Science* **304**, 847 (2004)
- [64] D. G. A. L. Aarts and H. N. W. Lekkerkerker, *J. Phys.: Condens. Matter* **16**, S4231 (2004)
- [65] S. Asakura and F. Oosawa, *J. Chem. Phys.* **22**, 1255 (1954)
- [66] A. Vrij, *Pure Appl. Chem.* **48**, 471 (1976)
- [67] R. L. C. Vink and J. Horbach, *J. Chem. Phys.* **121**, 3253 (2004); R. L. C. Vink, in *Computer Simulation Studies in Condensed Matter Physics XVIII*, eds. D.P. Landau, S.P. Lewis, and H.B. Schuettler (Springer Verlag, Heidelberg, Berlin, 2004)
- [68] R. L. C. Vink and J. Horbach, *J. Phys.: Condens. Matter* **16**, S3807 (2004); R. L. C. Vink, J. Horbach, and K. Binder, *Phys. Rev. E* **71**, 011401 (2005)
- [69] R. L. C. Vink, J. Horbach, and K. Binder, *J. Chem. Phys.* **122**, 134905 (2005)
- [70] R. J. Baxter, *Exactly Solved Models in Statistical Mechanics* (Academic Press, London, 1982)
- [71] J. W. Cahn, *J. Chem. Phys.* **66**, 3667 (1977)
- [72] D. E. Sullivan and M. M. Telo da Gama, in Ref. 12, p. 45
- [73] S. Dietrich, in *Phase Transitions and Critical Phenomena*, Vol XII, edited by C. Domb and J. L. Lebowitz, p. 1 (Academic Press, New York, 1988)
- [74] M. Schick, in Ref. 13, p. 415
- [75] J. Zinn-Justin, *Phys. Repts.* **344**, 159 (2001)
- [76] K. Binder and E. Luijten, *Phys. Repts.* **344**, 179 (2001)
- [77] K. Binder, in *Phase Transition and Critical Phenomena*, Vol. 8, edited by C. Domb and J. L. Lebowitz, p. 1 (Academic Press, New York, 1983)

- [78] M. E. Fisher, in *Critical Phenomena*, edited by M. S. Green (Academic Press, New York, 1971) p. 1
- [79] M. N. Barber, in *Phase Transitions and Critical Phenomena, Vol. 8*, edited by C. Domb and J. L. Lebowitz (Academic Press, New York, 1983) p. 145
- [80] V. Privman (ed.) *Finite Size Scaling and Numerical Simulation of Statistical Systems* (World Scientific, Singapore, 1990)
- [81] K. Binder, in *Computational Methods in Field Theory*, edited by C. B. Lang and H. Gausterer (Springer, Berlin, 1992), p. 59.
- [82] E. Luijten and H. Meyer, Phys. Rev. E **62**, 3257 (2000)
- [83] E. Luijten and K. Binder, Phys. Rev. E **58**, 4060(R) (1998)
- [84] M. A. Anisimov, E. Luijten, V. A. Agayan, J. V. Sengers and K. Binder, Phys. Lett. A **63**, 264 (1999)
- [85] P. Virnau and M. Müller, J. Chem. Phys. **120**, 10925 (2004)
- [86] K. Binder and D. P. Landau, Phys. Rev. B **30**, 1477 (1984); C. Borgs and S. Kappler, Phys. Lett. A **171**, 37 (1992); M. Müller and N. B. Wilding, Phys. Rev. E **51**, 2079 (1995)
- [87] K. Binder, Phys. Rev. A **25**, 1699 (1982)
- [88] K. Binder, Z. Phys. **B43**, 119 (1981)
- [89] G. Kamieniarz and H. W. J. Blöte, J. Phys. A: Math. Gen. **26**, 201 (1993)
- [90] M. E. Fisher and S.-Y. Zinn, J. Phys. A: Math. Gen. **31**, L629 (1998)
- [91] N. Wilding, in *Annual Reviews of Computational Physics*, edited by D. Stauffer (World Scientific, Singapore, 1996), p. 37.
- [92] D. Nicolaides and A. D. Bruce, J. Phys. A **21**, 233 (1988); A. D. Bruce and N. B. Wilding, Phys. Rev. Lett. **68**, 193 (1992)
- [93] J. Potoff and A. Panagiotopoulos, J. Chem. Phys. **112**, 6411 (2000)
- [94] B. A. Berg, U. Hansmann, and T. Neuhaus, Phys. Rev. B **47**, 497 (1993)
- [95] Y. C. Kim, M. E. Fisher and E. Luijten, Phys. Rev. Lett. **91**, 065701 (2003); Y. C. Kim and M. E. Fisher, Comput. Phys. Commun. **169**, 295 (2005); Y. C. Kim, Phys. Rev. E **71** 051501 (2005)
- [96] Y. C. Kim and M. E. Fisher, Phys. Rev. E **68**, 041506 (2003)
- [97] A. M. Ferrenberg and R. H. Swendsen, Phys. Rev. Lett. **61**, 2635 (1988); A. M. Ferrenberg and R. H. Swendsen, Phys. Rev. Lett. **63**, 1195 (1989)
- [98] F. Lo Verso, R. L. C. Vink, D. Pini, and L. Reatto, in preparation (2006)
- [99] R. L. C. Vink, to appear in J. Chem. Phys. (2006), see also cond-mat/0601075
- [100] Y. C. Kim, M. E. Fisher and G. Orkoulas, Phys. Rev. E **67**, 061506 (2003)
- [101] I. Brovchenko, A. Geiger, and A. Oleinikova, Eur. Phys. J. B **44**, 345 (2005)